Case Studies in Thermal Engineering 38 (2022) 102354

Contents lists available at ScienceDirect

Case Studies in Thermal Engineering

journal homepage: www.elsevier.com/locate/csite

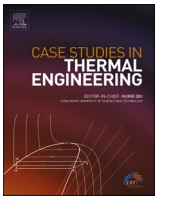

Optimising integrated heat spreaders with distributed heat transfer coefficients: A case study for CPU cooling

J.W. Elliott [a,b,*], M.T. Lebon [a,c], A.J. Robinson [a,b,c]

[a] Department of Mechanical, Manufacturing & Biomedical Engineering, Trinity College Dublin, Ireland
[b] AMBER Research Centre, Naughton Institute, Trinity College Dublin, Ireland
[c] Nexalus Ltd. Unit 13, South Bank, Crosse's Green, Cork, Ireland

ARTICLE INFO

Keywords:
Heat spreader
Conjugate heat transfer
Electronics cooling

ABSTRACT

Increasing power densities of modern CPUs has led to regions of high temperature on the semiconductor die which can lead to performance and reliability problems. In this case study, the effect of imposing a non-uniform heat transfer coefficient profile across the convective surface the CPU's integrated heat spreader was investigated as a potential enhanced cooling concept. A finite element model of a copper heat spreader of 40 × 40 mm^2 area and 2.5 mm thickness with a centred 13 × 13 mm^2 heat source at 100 W/cm^2 heat flux was considered to approximate typical modern high-powered CPUs. Both uniform and Gaussian distributions of the heat transfer coefficient were then considered. For the latter, both single and multi-objective Genetic Algorithm optimisation were carried out for three source temperature objectives; average temperature, maximum temperature and maximum temperature difference. The analysis showed that the multi-objective optimisation strategy produced the best overall heat transfer coefficient distribution, with almost 5 K reduction in both the maximum temperature and temperature gradient across the heat source compared with a uniform heat transfer coefficient distribution.

1. Introduction

The increasing power densities of central processing units (CPUs) has led to regions of high heat flux on the semiconductor die. The concentration of thermal power can negatively influence CPU performance, to the point that thermal management can dictate the design power. Practically, if cores on the CPU die exceed the maximum specified temperature threshold, it causes the performance of the CPU to be throttled in order to reduce power and prevent damage [1]. In multicore processors, uneven distribution of compute activity can lead to uneven heat flux distribution, which can exacerbate cooling challenges [2]. Therefore, it is imperative that adequate cooling is available, specifically for the hottest and most problematic core(s) on the silicon die. Further to this, aggressive global cooling to target the problem core(s) may overcool neighbouring cores, leading to significant temperature gradients on the die, which presents its own reliability problems [3]. As such, advanced cooling of CPUs must consider a balance that enables adequate cooling of the hottest core(s), yet not induce unacceptable thermal gradients along the die.

The cooling effectiveness of a concentrated heat source can be improved by spreading the thermal energy to a larger convective cooling area, effectively increasing the area of convective heat transfer with associated reduction in its thermal resistance. In CPU packages, this is facilitated by incorporating an Integrated Heat Spreader (IHS) between the die and the convective heat sink. Thermal

* Corresponding author. Department of Mechanical, Manufacturing & Biomedical Engineering, Trinity College Dublin, Ireland.
E-mail address: joelliot@tcd.ie (J.W. Elliott).

https://doi.org/10.1016/j.csite.2022.102354
Received 22 May 2022; Received in revised form 9 July 2022; Accepted 5 August 2022
Available online 12 August 2022

management of the electronic package thus requires accurate determination of individual thermal resistances present between contacting surfaces for the system in question, including the IHS [4]. Robinson et al. [5] determined that, for a concentrated heat source, increasing the size of the IHS lateral dimension can indeed decrease the convective and overall resistance. However, this decreasing trend plateaus such that little benefit is achieved for high IHS sizes. Similarly, if the lateral dimension of the spreader is fixed, an optimal IHS thickness exists which minimises the characteristic temperature (maximum or average) of the heat source [6]. Although increased thickness tends to improve lateral conduction, it simultaneously increases the transverse conduction resistance. It is therefore vital that, for a given heat source, the IHS dimensions are considered critically and optimised, with the aim of minimising the spreader thermal resistance or maximising its effective conductance [7]. If designed correctly, the additional resistance associated with the IHS system will be more than offset by the reduced convective resistance, leading to an overall reduction in the source-to-sink thermal resistance, facilitating cooler die temperatures or potentially reduced coolant flow rate for the same cooling effectiveness [8,9].

In order to optimise an IHS system, prediction of the thermal resistance associated with a concentrated source on a heat spreader with a convective boundary condition on the opposite face is required. Most cooling strategies can be well approximated as a uniform convective resistance on the cooled surface, which is a sufficient simplification to allow analytic modelling of the 3-dimensional heat flow problem. Exact and approximate analytic solutions have been put forth by several authors, including but not limited to Refs. [10–17], with a detailed review provided by Razavi et al. [18]. Of the available analytic solutions, the model proposed by Lee at al [19]. is the most convenient, owing to the leading order approximation eliminating the infinite series terms, and has been shown to be very accurate [12]. In the context of aggressive cooling of high-powered CPUs, the analytic models show that increasing the effective heat transfer coefficient decreases the source-to-sink thermal resistance. Although this is unsurprising, it is noted that this is a conjugate heat transfer problem, so the optimum IHS dimensions will also be sensitive to the imposed convective boundary condition.

As CPU heat fluxes escalate, cooling with air becomes less feasible owing to issues around fan power, noise, compactness and inadequate cooling effectiveness. In applications such as in data centres, which can host thousands of CPUs, the infrastructure energy associated with conditioning and handling air, along with the low potential for heat recovery, also become problematic [20,21]. The practical limitations of air cooling have motivated an emerging shift to liquid cooling of CPUs owing to its superior thermophysical properties [22]. A large body of work has been published on advanced liquid cooling technologies that include though is not limited to microchannels [23], pin fins [24], microjets [25,26], and hybrid solutions [27]. As mentioned, however, aggressive liquid cooling will influence the heat flow in the IHS owing to the conjugate nature of the problem. Liquid cooling solutions and concepts that specifically target concentrated heat sources are less common. The works of Kim et al. [7], Nikolić et al. [28], Lee at al. [29], Sharma et al. [30], Laguna et al. [31], Wu et al. [32] Wiriyasart & Naphon [33] and Kong et al. [34], are examples of liquid cooling studies that consider concentrated heat sources and both the convection and conduction problem simultaneously. An important conclusion that can be drawn from these studies is that clever design of the liquid cooled heat sink can positively influence the source-to-sink resistance of the package, including target cooling of hot spots.

It is evident from the literature that the concepts of heat spreading and high-performance liquid cooling have been extensively investigated. The preponderance of knowledge is associated with the scenario whereby the heat transfer coefficient across the heat spreader is uniform. Less work has been conducted on the combined conductive-convective problem, though there is evidence that hot spot mitigation occurs when concentrating the convective heat transfer in regions of high heat flux. In other words, when a concentrated heat source is dissipating heat through an IHS, providing a heat transfer coefficient that is non-uniform on the cooled face is likely to be advantageous.

The aim of this case study is to investigate the effect of aggressive cooling solutions which incorporate non-uniform heat transfer coefficient distributions on the convective surface of an IHS in order to determine if a significant improvement in thermal performance

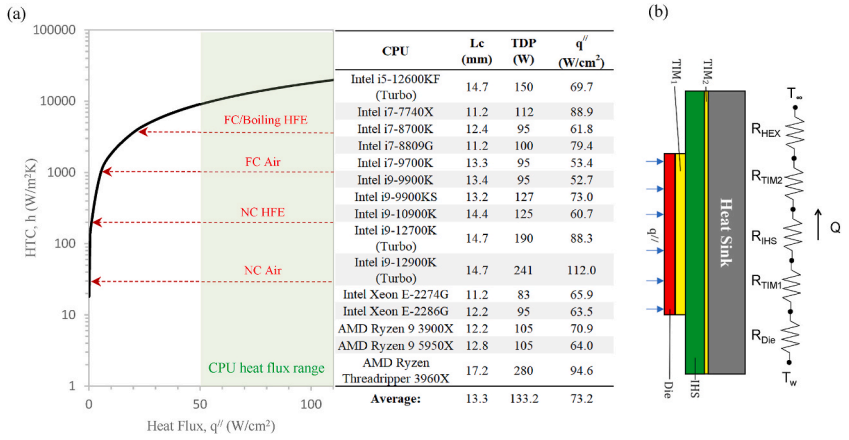

CPU	Lc (mm)	TDP (W)	q'' (W/cm²)
Intel i5-12600KF (Turbo)	14.7	150	69.7
Intel i7-7740X	11.2	112	88.9
Intel i7-8700K	12.4	95	61.8
Intel i7-8809G	11.2	100	79.4
Intel i7-9700K	13.3	95	53.4
Intel i9-9900K	13.4	95	52.7
Intel i9-9900KS	13.2	127	73.0
Intel i9-10900K	14.4	125	60.7
Intel i9-12700K (Turbo)	14.7	190	88.3
Intel i9-12900K (Turbo)	14.7	241	112.0
Intel Xeon E-2274G	11.2	83	65.9
Intel Xeon E-2286G	12.2	95	63.5
AMD Ryzen 9 3900X	12.2	105	70.9
AMD Ryzen 9 5950X	12.8	105	64.0
AMD Ryzen Threadripper 3960X	17.2	280	94.6
Average:	13.3	133.2	73.2

Fig. 1. **(a)** Required convective heat transfer coefficient versus heat flux for a 13 mm square die and required source-to-sink temperature difference of $\Delta T_{j\text{-}c} = 55$ K, along with approximate magnitudes of direct contact convection of insulating coolants. Inset table provides list of typical modern high heat flux CPUs. **(b)** Illustration of the thermal stack with associated thermal resistance diagram of a CPU package.

is realised compared with a uniform distribution. To achieve this, a realistic case study scenario, typifying modern CPUs, has been chosen. A non-uniform Gaussian distribution function of the convective heat transfer coefficient was then optimised by considering different temperature objectives to determine the best thermal performance. Although this case study targets a single CPU architecture with uniform thermal loading at the source and specific functional form of the convective heat transfer coefficient, the mathematical process developed can be adapted to broader and more complex scenarios, including different geometric configurations, non-uniform heat loading and multi-chip modules.

2. Heat spreaders in modern CPU packages

2.1. Why are heat spreaders required in modern CPUs?

The embedded table in Fig. 1(a) presents an example list of modern high heat flux CPUs available from Intel and AMD, where the appropriate die characteristic dimension has been determined from the die area ($l_c = \sqrt{A_{die}}$) [35] and the heat flux determined from A_{die} and the manufacturer-recommended Thermal Design Power ($q'' = Q_{TDP}/A_{die}$). The heat fluxes of the selected CPUs range between around 50 W/cm^2 to over 110 W/cm^2, and this can be considered conservative, since the CPU cores occupy only a region of the total lower die surface. For illustrative purposes in this case study, the average characteristic size of $l_c = 13$ mm will be used for a square die as representative of high heat flux CPUs.

Fig. 1(a) illustrates how the required heat transfer coefficient, ($h = q''/\Delta T_{j\text{-}c}$) varies with the heat flux, q'', when a source-to-sink temperature difference of $\Delta T_{j\text{-}c} = T_j\text{-}T_c = 55\ K$ must be maintained. This corresponds with a maximum allowable junction temperature of $T_j = 90°C$ at the source, typical of modern CPUs, and a coolant temperature of $T_c = 35°C$, which is the suggested heat sink design temperature for CPUs [36]. The figure also compares the approximate achievable heat transfer coefficient magnitudes of different direct contact natural convection (NC) and forced convection (FC) types, for air and a typical dielectric liquid (here HFE7000), with that required to sufficiently cool the bare CPU die. As shown, even with boiling of a refrigerant on the die, direct cooling is clearly incapable of achieving sufficient heat transfer coefficients to cool modern CPUs [37]. Consequently, engineering solutions must be implemented to decrease the thermal resistance and thus facilitate cooling with air and dielectrics, or potentially allow use of more effective heat transfer fluids, like water.

The relationship for convective thermal resistance, $R_{conv} = (hA_{IHS})^{-1}$, indicates that the thermal resistance is inversely proportional to the surface area. Consequently, for a given convective heat transfer intensity, R_{conv} can be decreased by increasing the total surface area upon which convection acts. In modern CPUs packages, this is facilitated via the introduction of an Integrated Heat Spreader (IHS), as depicted in Fig. 1(b). An IHS functions by adding additional surface area between the heat source and the heat sink, allowing the heat to spread laterally. Hence, for an otherwise insufficient convective heat transfer coefficient, h, there can be enough surface area, A_{IHS}, to allow the target thermal resistance to be achieved. Practically, however, implementing an IHS requires the stack package depicted in Fig. 1(b), and involves the penalties of adding further resistances to the thermal network, namely the Thermal Interface Materials (TIMs) and the IHS itself. The balance, when adding these elements to improve the heat transfer, should always be to ensure that the net resistance is lower than if direct cooling occurred on the bare die. The inclusion of an IHS can be of further benefit as it acts as a protective barrier between the die and the coolant. Consequently, this allows the use of high-performance coolants, i.e. liquids like water, and high-performance thermal hardware, such as microchannels and microjet coldplates.

2.2. Integrated heat spreader thermal resistance

With the integration of an IHS into the package and its potential to facilitate a wide range of cooling options, a question then arises around how large R_{IHS} is in proportion to the thermal resistances that can be achieved by different practical heat sinks for various CPUs. To address this question, a straight-forward numerical model has been developed as a case study that is representative of modern high heat flux CPUs. Fig. 2(a) presents the geometry used for this IHS model, with area of 40 × 40 mm^2, thickness d, and a centrally located CPU die of 13 × 13 mm^2. When modelling the IHS, copper was selected as the material, with a thermal conductivity of $k = 400$ W/mK. The parameter ranges investigated were; effective heat sink conductance of 1000 W/m^{2}K $\leq h_{eff} \leq$ 50,000 W/m^{2}K, and IHS thickness between 1.0 mm $\leq d \leq$ 5.0 mm. These cases, where the convective heat transfer coefficient is uniform, can be considered the baseline to which the non-uniform scenarios will be compared in a later section.

The thermal model used to simulate the case study was based upon the steady state three-dimensional heat conduction equation, which assumes a constant thermal conductivity in the solid domain,

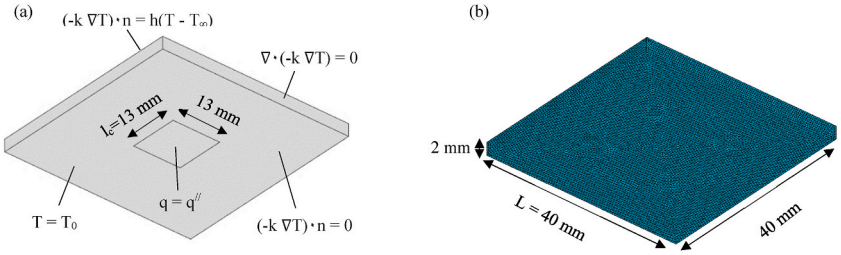

Fig. 2. (a) 3D geometry of IHS and heat source with associated boundary conditions. **(b)** 3D mesh of IHS geometry with dimensions.

$$\frac{\delta^2 T}{\delta x^2}+\frac{\delta^2 T}{\delta y^2}+\frac{\delta^2 T}{\delta z^2}=0 \tag{1}$$

where T is the temperature within the solid. This governing equation was subject to the following boundary conditions;

$$\frac{\delta T}{\delta x}|_{x=-\frac{L}{2}}=\frac{\delta T}{\delta x}|_{x=\frac{L}{2}}=\frac{\delta T}{\delta x}|_{y=-\frac{L}{2}}=\frac{\delta T}{\delta y}|_{y=\frac{L}{2}}=0 \tag{2}$$

$$-k\frac{\delta T}{\delta x}|_{z=d}=h(T-T_\infty) \tag{3}$$

$$k\frac{\delta T}{\delta x}|_{z=0}=\begin{cases} q'' & (x,y)\in\left(-\frac{l_c}{2},\frac{l_c}{2}\right) \\ 0 & (x,y)\in\left(-\frac{(L-l_c)}{2},\frac{(L-l_c)}{2}\right)\end{cases} \tag{4}$$

Here, h is the uniform convective heat transfer coefficient applied to the top surface, q'' is the uniform heat flux applied to the smaller area on the lower surface, $\frac{1}{2}L$ is half the length of the heat spreader and $\frac{1}{2}l_c$ is the half the length of the heat source, where the geometric model is constructed such that the centre of the square heat source is the origin.

The model used to simulate the heat transfer in the IHS was solved in the Matlab Finite Element solver using the Partial Differential Equation Toolbox. The MATLAB solver used triangular mesh elements, as depicted in Fig. 2(b), and mesh independence was verified by increasing the mesh density for a high heat flux ($q'' = 100$ W/cm^2) from 800,000 mesh elements, where the percentage error with the successive mesh was 7.24%, until the percentage error between successive simulations dropped below 1%, which occurred at 2.4 million mesh elements with an error of 0.89%.

The numerical simulation outputs for the non-uniform temperature distribution in the solid domain. The average net thermal resistance is typically presented as the sum of those associated with the heat spreader and convective heat transfer from the top face [4, 16,19];

$$R_{net,avg}=\frac{\overline{T}_{hs}-T_\infty}{Q}=R_{IHS}+\frac{1}{hA_{IHS}} \tag{5}$$

where $\overline{T}_{hs}$ is the average temperature of the heat source area, A_{die}, and R_{IHS} is the overall resistance associated with the addition of the heat spreader. Albeit convenient from a simplified calculation standpoint, to some degree it masks the true influence of the heat spreader by lumping it into the R_{IHS} term, where in fact both the conductive and convective heat transfer are influenced by the presence of the spreader. This is clearly observable in the investigation of Lee et al. [16] though not discussed explicitly.

Heat spreaders are, in principle, lateral fins since they are intended to increase the heat transfer surface area, precisely the function of traditional fins, though in a different orientation in relation to the heat source. However, they are not historically considered in the same manner as fins. Fins themselves are a classical scenario of conjugate heat transfer, where the solid phase conductive heat transfer is strongly dependant on the convective heat transfer that acts on the solid boundaries. This is also the case for heat spreaders and is an important consideration since, like fins, a heat spreader's purpose is to increase the surface area for convection to act. Therefore, considering the heat spreader as a fin can provide a more effective means to describe the conjugate heat transfer problem being considered.

The efficiency of the heat spreader can be defined in the same manner as the fin efficiency, which compares the thermal resistance to one of an infinite thermal conductivity.

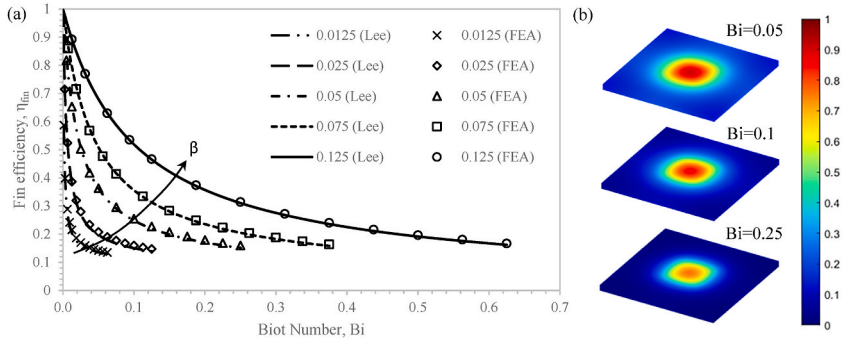

Fig. 3. **(a)** Comparison between fin efficiency versus Biot number for varying $\beta = d/L$. Also shown is the comparison between the current numerical simulations and the analytic solution of Lee et al. [19]. **(b)** Non-dimensional temperature distributions at different Biot numbers for $\beta = 0.05$.

$$\eta_{IHS} = \left(\frac{\frac{1}{R_{net,avg}}}{\frac{1}{hA_{IHS}}} \right) \tag{6}$$

where A_{IHS} is the surface area of the convective surface on the spreader. The spreader efficiency, η_{IHS}, thus provides a representation of the heat spreading performance, where the closer η_{IHS} is to unity, the more effective area of the spreader's top surface is active for convection to act. Consequently, the source-to-sink thermal resistance can be given by,

$$R_{net,avg} = (\eta_{IHS} A_{IHS}) h \tag{7}$$

Fig. 3(a) illustrates the relationship between the fin efficiency and the lateral Biot number $(Bi = hd/k)$ for different non-dimensional heat spreader thickness ratios, $\beta = d/L$. As this case study considers a fixed thermal conductivity, decreasing Bi is associated with decreasing convective heat transfer coefficient and vice versa. In terms of the analogy with traditional fins, this is the same behaviour with respect to heat transfer coefficient and fin efficiency. This is clearly depicted in Fig. 3(b), which plots distributions of the non-dimensional temperature, θ, for four different Biot numbers and $\beta = 0.05$, where,

$$\theta = \frac{T(x,y,z) - T_{\infty}}{T_{max} - T_{\infty}} \tag{8}$$

It is clear from Fig. 3(b) that the active area on the convective side of the IHS decreases with increasing magnitude of Bi, consistent with the lower calculated spreader efficiency. It is also clear from Fig. 3(a) that decreasing the thickness of the spreader, which restricts the lateral heat transfer, decreases the overall spreader efficiency, in the same manner as traditional fins. Also shown in Fig. 3(a) is the comparison between the present FEA numerical model and the approximate analytical model of Lee et al. [19]. The figure indicates that the numerical model is capable of adequately reproducing the analytical data and gives confidence in the efficacy of both modelling approaches.

The key point here is that, like traditional fins, the conductive heat transfer in solid heat spreaders is highly coupled with the convective heat transfer. When implementing aggressive cooling that globally cools the top surface, such as with water-cooled coldplates, the drop in spreader efficiency means that the effective area of convective cooling is small. This is not ideal and brings into question whether global-cooling the surface of the IHS is the best option. Pumped water-cooling loops in computing systems have constraints on pressure drop and flow rate. It thus seems better engineering judgement to deploy the limited coolant resource to the portions of the heat sink that are more actively heated. However, this being a conjugate heat transfer problem, focussing the convective heat transfer will influence the conductive heat transfer, requiring a full conjugate heat transfer analysis to explore the overall impact on the cooling effectiveness, combined with an optimisation strategy to find the best overall operating condition.

3. Distributed heat transfer coefficient distribution and optimisation strategy

3.1. Heat transfer coefficient distribution

Based on the position of the heat source relative to the spreader, the aim when considering the distribution of the heat transfer coefficient was to have a continuous function that contained a maximum located at the centre of the IHS convective surface, which would decrease to a non-zero value at the outer edges of the IHS. This would be similar to the behaviour of the temperature fields on the IHS convective surface as seen in the previous section. This concentration of the heat transfer coefficient at the centre would enable better lateral spreading across the IHS and help produce a more uniform temperature distribution across the convective surface.

Based on this logic, a Gaussian distribution was determined to be a suitable function, as it produces a centrally located maximum which decreases to a minimum on either side of the peak. The associated mathematical form of this function contains inputs which can be used to control the steepness of the peak region of the curve and the minimum value to which it decreases. These variables could therefore be tailored accordingly based on the heat flux applied at the source. The Gaussian function was specified as:

$$f(x) = \frac{1}{\sigma\sqrt{2\pi}} e^{-\frac{1}{2}\left(\frac{x-\mu}{\sigma}\right)^2} \tag{9}$$

where μ is the mean value of the data set and σ is the standard deviation. To maintain a certain level of control over the optimisation, a limit was introduced into the function that specifies the average heat transfer coefficient across the whole convective surface of the IHS. This allows the function to remain within practical limits of achievable convective heat transfer coefficients. To facilitate this, the Gaussian function was amended as,

$$f(x) = \left(Z\, e^{-\frac{1}{2}\left(\frac{x}{a}\right)^2} \right) + m \tag{10}$$

Here, m is the minimum heat transfer coefficient that the curve asymptotically approaches in the far-field, and a is a multiplier that controls the width of the peak curve, which falls within the limits of 0.001–0.01. The expression for Z is specified as,

$$Z = \frac{2\sqrt{2}\,(h_{avg} - m)}{\sqrt{\pi}\,a\left(\mathrm{erf}\left(\frac{r}{\sqrt{2}\,a}\right)\right) - \mathrm{erf}\left(\frac{-r}{\sqrt{2}\,a}\right)} \tag{11}$$

where h_{avg} is the specified average heat transfer coefficient magnitude across the entire convective surface, and r is the displacement from the origin, here the centre of the IHS. The Gauss error function is defined as [38],

$$erf : x \Big| \rightarrow \frac{2}{\sqrt{\pi}} \int_0^x e^{-v^2}\, dv \tag{12}$$

Fig. 4 illustrates how the variable inputs *a* and *m* affect the overall Gaussian distribution, where an increasing value of *a* produces a broader curve and reduces the maximum value of the peak to maintain the specified average, while increasing *m* increases the minimum value reached by the asymptotes in the far-field. An increase in *m* also contributes to a reduction in the maximum peak value, again to maintain the convective surface average heat transfer coefficient condition.

3.2. Heat transfer coefficient optimisation

3.2.1. Objective functions and variable inputs parameters

For this case study, the main area of concern was the contact area between the heat source and solid heat spreader, since this is the location where the CPU die interfaces with the IHS and is the location where the highest temperatures are located. The temperature profile of the heat source region can be characterised by three different temperatures: the average temperature, T_{avg}, which indicates the overall effectiveness of the cooling solution; the maximum temperature, T_{max}, which represents the most problematic region of the source; and the temperature difference, $\Delta T_{max\text{-}min}$, which is indicative of the temperature gradients and thus thermal stresses which would be present across the die-IHS interface. These three temperatures were considered as the objective functions.

Two inputs were set as variable parameters during optimisation: the minimum far field heat transfer coefficient, *m*, and the peak curve width indicator, *a*. The input for the former was confined to a range of $0 \leq m \leq 30{,}000$ W/m^{2}K, whereas the latter was set between $0.001 \leq a \leq 0.01$. The other geometric parameters, physical properties and boundary conditions were considered to be constant for this example case study: $q'' = 100$ W/cm^2, $A_{Die} = 13 \times 13$ mm^2, $A_{IHS} = 40 \times 40$ mm^2, $b = 2.5$ mm, and $k = 400$ W/mK. The average heat transfer coefficient condition was set at a constant value of $h_{avg} = 35{,}000$ W/m^{2}K. In terms of overall heat transfer coefficient, this magnitude is in line with those achievable by both microjet impingement and microchannel based heat exchangers [22]. The influence of a Thermal Interface Material was accounted for by assuming a 0.1 mm thickness of 3.0 W/mK thermal grease between the die and IHS.

3.2.2. Genetic algorithm

An in-house Genetic Algorithm (GA) program was written using the Matrix Laboratory R2022a optimisation toolbox in Matlab. GA utilises an optimisation strategy based on natural selection evolution via genetic reproduction, mutation and crossover. The algorithm uses the individuals from the previous generation to create the children that make up the current generation. This iterative process is run until a global optimum for the specified objective function(s) is found [39]. The rate of mutation for this case study was set as *adaptive*, implying that during the optimisation process, each iteration randomly combines genes of individuals from the previous iteration to form new children. This process then adapts with each successive generation based on the results of the last. For a multi-objective problem, this helps to ensure that the true global optimum is located as opposed to a localised optimum, which can miss sections of the test range [40]. Table 1 presents the GA parameters used for the case study.

4. Results and discussion

For a case study, the methodology and potential impact of the type of design intervention are presented for a specific design scenario. In a real-world context, a case study is performed in preference to investigating all the possible scenarios that could be encountered, as these would be too numerous. Thus, an 'average CPU' is considered, in the sense that the fixed parameters listed in

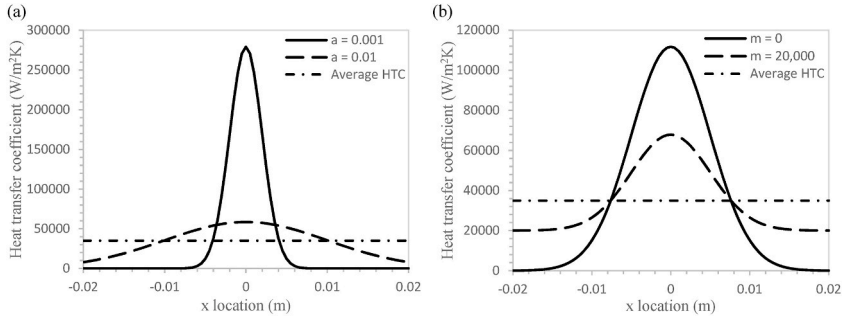

Fig. 4. Gaussian convective heat transfer coefficient distribution profiles showing the effects of changing the inputs *a* and *m* with a surface average of $h_{avg} = 35{,}000$ W/m^{2}K. **(a)** Constant $m = 0$ W/m^{2}K for different values of *a*, **(b)** Constant $a = 0.05$ for varying *m*.

Table 1
Genetic algorithm operating parameters.

Operating parameter	Value
Objective Functions	3
Variable Inputs	2
Initial population size	50
Max. Generations	1000
Crossover fraction	0.8
Mutation	Adaptive

Table 2
Case study fixed parameter values.

Parameter	Symbol	Value	Unit
Heat spreader length	l_c	13	mm
IHS length	L	40	mm
IHS thickness	d	2.5	mm
Thermal conductivity	k	400	W/mK
Average heat transfer coefficient	h_{avg}	35,000	W/m^2K
Heat flux	q''	100	W/cm^2
Ambient Temperature	T_c	35	°C

Table 2 used in this case study were informed by existing commercial CPU packages (Fig. 1).

4.1. Baseline global cooling case

In order to provide context for later comparisons, Fig. 5(b) and (c) presents the local and distribution of the temperatures across the IHS associated with the baseline case, where a uniform heat transfer coefficient of $h_{avg} = 35{,}000$ W/m^2K was applied across the convective surface of the IHS (Fig. 5 (a)). For this case, $Bi = 0.219$ and $\beta = 0.0625$. The maximum temperature, $T_{max} = 87.4$ °C occurs at the geometric centre of the heat source on the bottom surface, as clearly illustrated in Fig. 5(b). The temperature differential across the heat source/IHS contact area is $\Delta T_{max\text{-}min} = 11.7$ K and the average temperature of the heat source was calculated to be $T_{avg} = 83.3$ °C.

The top and bottom temperature profiles are such that the temperature decreases monotonically from the geometric centre of the spreader to a slope of zero at the edge, owing to the adiabatic boundary condition imposed there. It can be seen from Fig. 5 (b) that an inflection point occurs at the approximate location of the heat source edge (x/L = 0.325) on the bottom surface of the IHS, as the curves change from being concave to convex beyond this point. This prompts high temperature gradients, and subsequent lateral heat conduction, in this location, which diminish to zero at the edge of the IHS.

For this baseline case, the spreading efficiency of the IHS was found to be $\eta_{IHS} = 0.21\%$, implying that only a fifth of the available heat spreader surface area was effectively active for convective heat transfer. Considering the 2D temperature distributions displayed

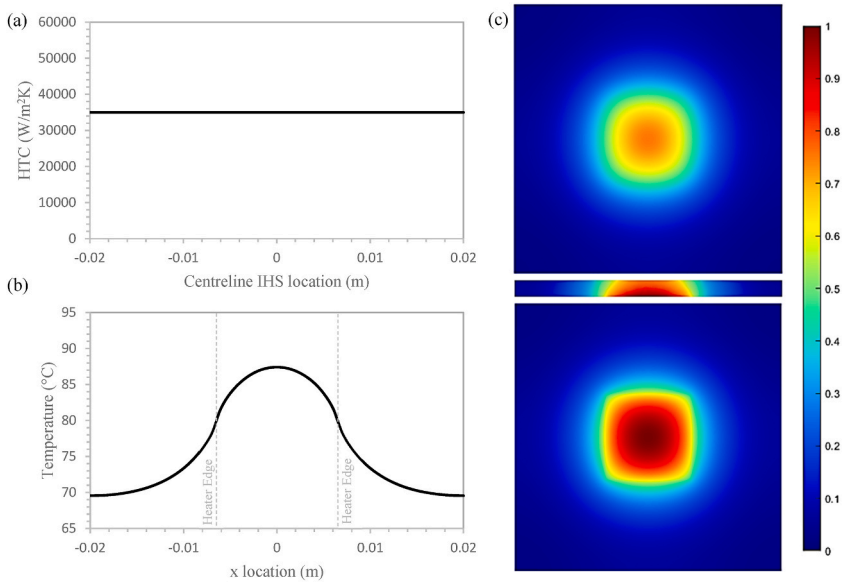

Fig. 5. (a) Plot of convective heat transfer coefficient distribution on top surface, **(b)** plot of centreline temperature distribution on bottom surface, and **(c)** non-dimensional temperature distribution (Top) convective side, (Middle) centreline cross-section, (Bottom) heat source side.

in Fig. 5(c), it is evident that this low efficiency is due to the lack of lateral heat spreading across the IHS. Conversely, the thermal energy remains concentrated directly above the heat source, with most of the heat flowing transversely in the region of the heat source. Since the convective heat flux at the top surface is proportional to the difference in wall and coolant temperature at the surface, $q''_{conv} \propto T(x,y,b) - T_c$, the distribution in the top image of Fig. 5(c) is indicative of the convective heat flux distribution, which is clearly localised.

4.2. Optimised convective cooling cases

As shown in Fig. 6(a), the optimal convective heat transfer distributions for T_{max} and each T_{avg}, T_{max} and $\Delta T_{max\text{-}min}$ (cases (ii) and (iii)) are broadly similar and fall in between the more extreme profiles of cases (iv) and (v) that optimised for the T_{avg} and $\Delta T_{max\text{-}min}$ objective functions respectively. Consequently, the temperature distributions for case (ii) and (iii) are very similar, as shown qualitatively in Fig. 6(b) and more qualitatively in the centreline temperature plots in Fig. 7. As a result, the improvements in the performance metrics over the baseline case, (T_{avg}-$T_{avg,case\ (i)}$), (T_{max}-$T_{max,case\ (i)}$), ($\Delta T_{max\text{-}min}$ - $\Delta T_{max\text{-}min,\ case\ (i)}$), shown in Fig. 8, do not differ significantly whether T_{max} or each ΔT_{avg}, T_{max} and $\Delta T_{max\text{-}min}$ are chosen as the objective functions. Importantly, the concept proposed here, that a distributed heat transfer coefficient can provide superior cooling performance of heat spreaders of otherwise low spreading efficiency, is proven. Although the average source temperature is only reduced by T_{avg}-$T_{avg,case\ (i)} = -1.2$ K for the multi-objective optimisation case (ii), the maximum temperature is decreased by T_{max}-$T_{max,case\ (i)} = -3.6$ K, and the temperature gradient diminished by $\Delta T_{max\text{-}min}$ - $\Delta T_{max\text{-}min,\ case\ (i)} = -5.2$ K, which are significant.

It is clear from Fig. 6(a) and (b) that a higher, and subsequently more focused, distribution of the heat transfer coefficient in the central region leads to a more uniform temperature across the IHS. Focussing the heat transfer coefficient acts to mitigate the lateral temperature gradients which would otherwise promote conduction from the centre of the IHS to the outer edges. This is apparent in Fig. 7, particularly for the $\Delta T_{max\text{-}min}$ optimisation case (v), which has the most focused heat transfer coefficient profile with the highest peak magnitude and subsequent most uniform non-dimensional temperature, θ, distribution that is comparatively closest to unity throughout most of the domain. Closer inspection of Fig. 7(a) reveals that the highly focussed heat transfer coefficient of this case has the effect of creating a local minimum in θ at the centre of the heat source, and a local maximum of slightly higher magnitude in the region of the heat source's edge (x/L = 0.325). This is the only case where the maximum temperature is not located at the geometric centre of the heat source. Similarly for the top surface of the IHS plotted in Fig. 7(b), the temperature gradients for case (v) are positive, i.e., directed inwards, denoting lateral conduction inward towards the centre. Consequently, to create a uniform temperature distribution on the localised heat source, such as the one considered here, requires sufficiently intense and focussed convective cooling in the source region to cause the lateral flow of heat in the solid to be directed inward towards the central region.

An interesting observation can be made by comparing case (v) to the baseline case (i) which is the non-focussed, uniform heat transfer coefficient scenario. Case (i) has the steepest temperature gradients which are directed outwards from the centre. This indicates that there is high lateral conduction across the IHS, where the spreader is conducting heat across the full extent of the spreader,

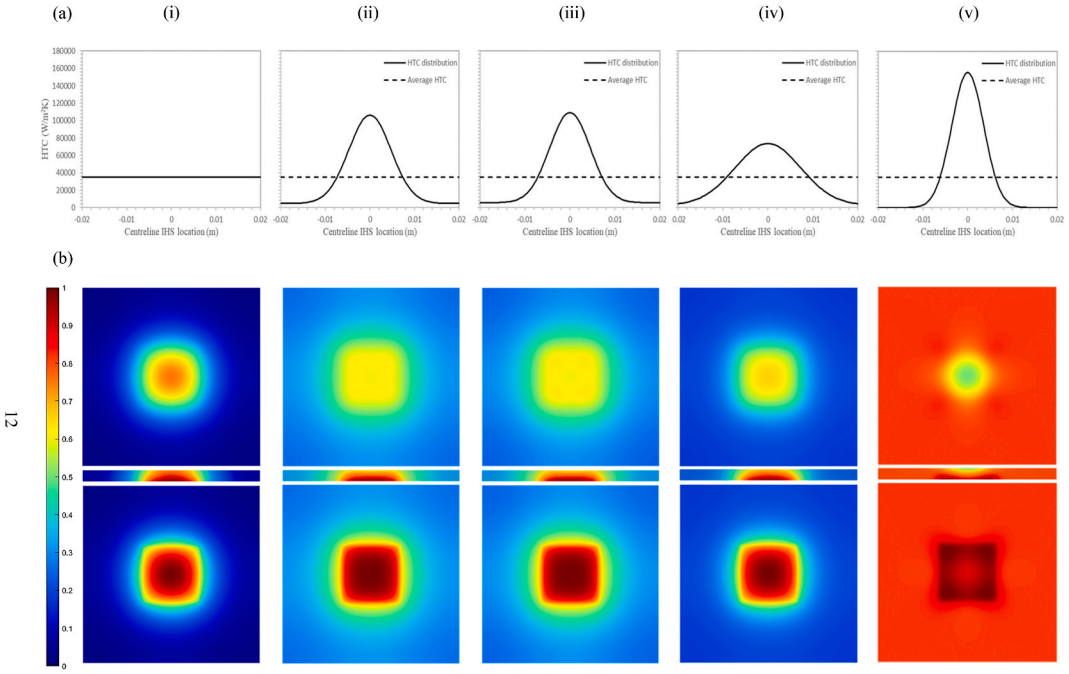

Fig. 6. (a) Plot of convective heat transfer coefficient distribution on top surface, (b) non-dimensional temperature distribution (Top) convective side, (Middle) centreline cross-section, (Bottom) heat source side. From left to right; (i) baseline global cooling case, (ii) multi-objective optimised for T_{avg}, T_{max}, $\Delta T_{max\text{-}min}$, and single objective optimised for (iii) T_{max}, (iv) T_{avg}, and (v) $\Delta T_{max\text{-}min}$.

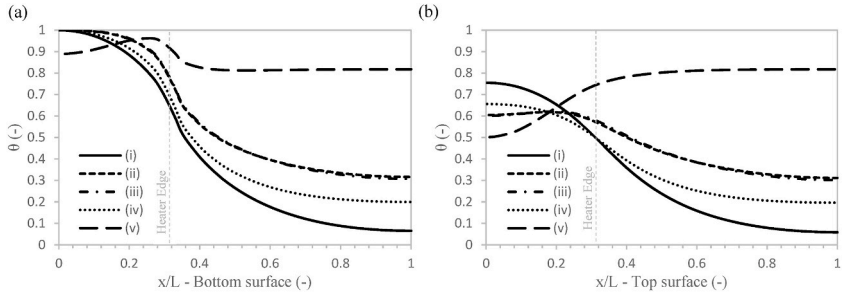

Fig. 7. Comparison of non-dimensional temperature profiles between the optimisation cases across; **(a)** the bottom surface and **(b)** the top surface for half the length of the IHS.

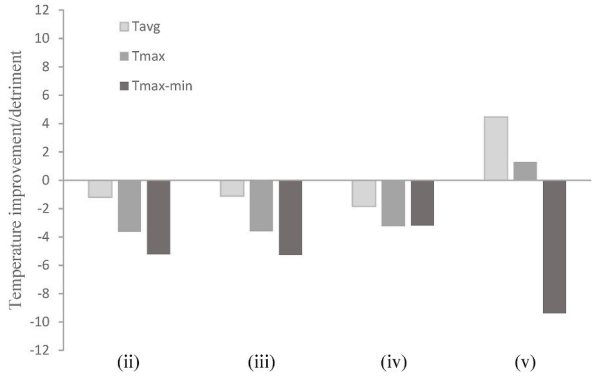

Fig. 8. Improvement or detriment in temperature performance metrics for each optimisation case compared to the baseline.

since convection is occurring to the edge of the spreader in this scenario. Conversely, for case (v), the optimum convective heat transfer coefficient distribution ostensibly insulates the spreader over a large portion of the area (Fig. 6(a)), forcing the heat to be dissipated in the central region. Here, $dT/dx \sim 0$ in the outer regions of the IHS on both the top and bottom surfaces, as seen in Fig. 7, such that minimal lateral conduction is occurring to the peripheral region, since there is no convective means to dissipate the heat. The consequence, however, is that the most uniform temperature gradient at the heat source ($\Delta T_{max\text{-}min}$ - $\Delta T_{max\text{-}min,\ case\ (i)} = -9.4$ K) is attained at the sacrifice of having increased T_{avg} and T_{max} levels compared to the baseline, as shown in Fig. 8. Here, T_{max}-$T_{max,case\ (i)} =$ 1.3 K, and T_{avg}-$T_{avg,case\ (i)} = 4.5$ K, both being detrimental in terms of overall performance.

Of the four optimisation cases studied, minimising T_{avg} (case (iv)) results in the least concentrated convective heat transfer coefficient distribution. Like the baseline case (i), the top and bottom temperature profiles are such that the slope is continuously negative and decreases monotonically from the geometric centre of the spreader to a slope of zero at the edge, owing to the adiabatic boundary condition imposed there. Unlike the baseline, the top surface temperature for case (iv) is suppressed in the central region owing to the elevated heat transfer coefficient, whilst both the top and bottom temperatures are sustained to a higher magnitude of θ in the far field, owing to the diminishing, yet non-zero, heat transfer coefficient. Thus, minimising T_{avg} requires a balance between increasing the convective heat transfer in the heated zone of the source whilst maintaining a degree of lateral conduction and subsequent convective cooling to the edge of the spreader. Overall, performance improvement over the baseline is reasonably good, with a 1.8 K drop in average temperature, with the added benefit of the maximum temperature and temperature gradient both improving by about 3.2 K.

Based on the evidence provided in Figs. 6–8, case (ii), the multi-objective optimisation case which minimises each of the objective functions ΔT_{avg}, T_{max} and $\Delta T_{max\text{-}min}$, can be said to be the best performing scenario. For this specific distribution function and under the prescribed conditions and constraints defined here, it strikes the best balance across all criteria for minimising temperatures across the heat source. The associated heat transfer coefficient distribution depicted in Fig. 6(a) is between the extremes cases (iv) and (v) i.e. the least and most concentrated respectively. Apparent from the non-zero temperature gradients in Fig. 7, lateral spreading is occurring to the edge of the spreader which remains heated, with $0.3 \lesssim \theta \lesssim 0.8$, in the far-field. This acts to sustain convective cooling over the entire spreader and subsequently lower the overall magnitude of the heat source temperature, consistent with case (iv) discussed above. Additionally, the distribution peak remains concentrated enough to maintain high convective heat flux heat directly above the heat source region, to the extent that the temperature gradient is slightly positive on the top surface above the source (Fig. 7(b)), signifying a reversal in the heat flow direction in this region. This aids in mitigating excessive temperature gradients across the source, consistent with case (v) discussed earlier. Fig. 6(b) illustrates these points, showing that the temperature distribution for case (ii) is reasonably concentrated in the region where the heat transfer coefficient is high, promoting high convective heat flux, yet sustains heating and associated convective heat flux, to the edge of the spreader. Fig. 8 reinforces how the improvement of all three temperature objectives

over the baseline for case (ii) falls between the results for the T_{max} and T_{avg} optimised cases, cases (iii) and (iv) respectively, indicating that the multi-objective optimisation scenario results in the best balance of criteria to provide the optimum cooling performance.

5. Conclusions

This case study has showed that the optimised non-uniform heat transfer coefficient function can realise significant reductions in both the operating temperature and the temperature gradients across the source compared with a uniform distribution. Other key findings from this investigation were as follows:

1. The steepest heat transfer coefficient profile occurred when minimising $\Delta T_{max\text{-}min}$ and produced the lowest temperature gradient across the heat source for the given heat flux, but at the cost of having overall higher average and maximum temperatures. The steeper and narrower profile discouraged outward lateral flow of heat, forcing transverse heat flow directly above the heat source. In fact, the lateral flow of heat was directed inward towards the centreline of the IHS in this case.
2. An optimum distribution of the heat transfer coefficient occurred for the multi-objective optimisation case where the objective functions T_{max}, T_{avg} and $\Delta T_{max\text{-}min}$ were minimised simultaneously. This provided a single result that balanced the gains achieved by each objective function individually.
3. Of the three single objective optimisation cases considered, minimising the maximum temperature of the heat source, T_{max}, was the best performing. Here, the resulting heat transfer coefficient distribution and performance enhancement were quite similar to the multi-objective optimum case. This potentially simplifies the mathematical optimisation process.

Given the findings of this case study, future research will focus on investigating the practical means to produce non-uniform distributions of the heat transfer coefficient via impinging liquid microjet array cooling, as it is capable of achieving the magnitudes of local heat transfer coefficient as calculated by this study [41].

Author statement

J. W. Elliott: Conceptualisation, Methodology, Software, Validation, Investigation, Data curation, Visualisation, Writing- Original draft preparation.

M. T. Lebon: Writing- Reviewing and Editing.

A. J. Robinson: Supervision.

Declaration of competing interest

The authors declare that they have no known competing financial interests or personal relationships that could have appeared to influence the work reported in this paper.

Data availability

Data will be made available on request.

Acknowledgments

This publication was developed with the financial support of Science Foundation Ireland (SFI) under grant number 12/RC/2278.

Nomenclature

l_c	Characteristic length of heat source (m)
A_{die}	Surface area of heat source (m^2)
L	IHS length (m)
d	IHS thickness (m)
A_{IHS}	Surface area of IHS (m^2)
T	Solid temperature (K)
T_∞	Atmospheric temperature (K)
T_c	Coolant temperature (K)
T_j	Junction temperature (K)
T_{max}	Maximum temperature at contact area between die and IHS (K)
T_{min}	Minimum temperature at contact area between die and IHS (K)
$\Delta T_{max\text{-}min}$	Temperature range across contact area between die and IHS (K)
T_{avg}	Average temperature of contact area between die and IHS (K)
$\overline{T}_{hs}$	Average temperature of heat source (K)
Q_{TDP}	Thermal design power (W)
q''	Heat flux (W/cm^2)
h	Heat transfer coefficient (W/m^2K)

h_{eff}	Effective heat sink conductance (W/m^2K)
h_{avg}	Average HTC profile across IHS convective surface (W/m^2K)
k	Thermal conductivity (W/mK)
R_{conv}	Convective thermal resistance (K/W)
R_{HEX}	Thermal resistance of heat exchanger (K/W)
R_{IHS}	Thermal resistance of IHS (K/W)
$R_{net,avg}$	Source-to-sink thermal resistance (K/W)
$\eta_{IHS'}$	Fin efficiency (%)
Bi	Biot number
m	Minimum HTC value of Gaussian distribution (W/m^2K)
a	Gaussian curve width indicator
erf	Gauss error function
x	IHS geometric location (m)
x/L	Non-dimensional IHS location

Greek Symbols

μ	Mean value of dataset
σ	Standard deviation of dataset
β	Non-dimensional heat spreader thickness ratio
θ	Non-dimensional temperature

Abbreviations

CPU	Central processing unit
FC	Forced convection
FEA	Finite element analysis
GA	Genetic algorithm
HEX	Heat exchanger
HTC	Heat transfer coefficient
IC	Integrated circuit
IHS	Integrated heat spreader
NC	Natural convection
TIM	Thermal interface material

References

[1] A.L. Moore, L. Shi, Emerging challenges and materials for thermal management of electronics, Mater. Today 17 (4) (2014) 163–174.
[2] L.S. Maganti, P. Dhar, T. Sundararajan, S.K. Das, Mitigating non-uniform heat generation induced hot spot(s) in multicore processors using nanofluids in parallel microchannels, Int. J. Therm. Sci. 125 (2018) 185–196.
[3] Y. Zhang, H. Wang, Z. Wang, Y. Yang, F. Blaabjerg, Simplified thermal modeling for IGBT modules with periodic power loss profiles in modular multilevel converters, IEEE Trans. Ind. Electron. 66 (3) (2019) 2323–2332.
[4] T.Q. Feng, J.L. Xu, An analytical solution of thermal resistance of cubic heat spreaders for electronic cooling, Appl. Therm. Eng. 24 (2–3) (2004) 323–337.
[5] A.J. Robinson, J. Colenbrander, R. Kempers, R. Chen, Solid and vapor chamber integrated heat spreaders: which to choose and why, IEEE Trans. Compon. Packag. Manuf. Technol. 8 (9) (2018) 1581–1592.
[6] G. Maranzana, I. Perry, D. Maillet, S. Raël, Design optimization of a spreader heat sink for power electronics, Int. J. Therm. Sci. 43 (1) (2004) 21–29.
[7] M. Kim, K.H. Lee, D.I. Han, J.H. Moon, Numerical case study and modelling for spreading thermal resistance and effective thermal conductivity for flat heat pipe, Case Stud. Therm. Eng. 31 (2022), 101803.
[8] M. Awad, A. Radwan, O. Abdelrehim, M. Emam, A.N. Shmroukh, M. Ahmed, Performance evaluation of concentrator photovoltaic systems integrated with a new jet impingement-microchannel heat sink and heat spreader, Sol. Energy 199 (2020) 852–863.
[9] A. Ali, Thermal performance and stress analysis of heat spreaders for immersion cooling applications, Appl. Therm. Eng. 181 (2020) 1359–4311.
[10] T.S. Fisher, F.A. Zell, K.K. Sikka, K.E. Torrance, Efficient heat transfer approximation for the chip-on-substrate problem, J. Electron. Packag. 118 (4) (1996) 271–279.
[11] M.M. Yovanovich, Y.S. Muzychka, J.R. Culham, Spreading resistance of isoflux rectangles and strips on compound flux channels, J. Thermophys. Heat Tran. 13 (4) (1999) 495–500.
[12] G.N. Ellison, Maximum thermal spreading resistance for rectangular sources and plates with nonunity aspect ratios, IEEE Trans. Compon. Packag. Technol. 26 (2) (2003) 439–454.
[13] T.Q. Feng, J.L. Xu, An analytical solution of thermal resistance of cubic heat spreaders for electronic cooling, Appl. Therm. Eng. 24 (2–3) (2004) 323–337.
[14] K. Alam, X. Shen, R. Taposh, in: Design Considerations for Heat Spreader in High Heat Flux Systems, *28th IEEE SEMI-THERM Symposium*, March 2012, pp. 18–22. San Jose, CA, USA.
[15] S.M. Thompson, H.B. Ma, Thermal spreading analysis of rectangular heat spreader, J. Heat Tran. 136 (2014), 064503.
[16] J. Lee, S.M. Thompson, T.E. Lacy Jr., Thermal spreading analysis of a transversely isotropic heat spreader, Int. J. Therm. Sci. 118 (2017) 461–474.
[17] H.A. Guo, K.F. Wiedenheft, C.H. Chen, Hotspot size effect on conductive heat spreading, IEEE Trans. Compon. Packag. Manuf. Technol. 7 (9) (2017), 1459-164.
[18] M. Razavi, Y.S. Muzychka, S. Kocabiyik, Review of advances in thermal spreading resistance problems, J. Thermophys. Heat Tran. 30 (4) (2016) 863–879.
[19] S. Lee, S. Song, V. Au, K.P. Moran, Constriction/spreading resistance model for electronics packaging, Proc. ASME/JSME Therm. Eng.Conf. 4 (1995) 199–206.
[20] S. Zimmermann, M.K. Tiwari, I. Meijer, S. Paredes, B. Michel, D. Poulikakos, Hot water cooled electronics: exergy analysis and waste heat reuse feasibility, Int. J. Heat Mass Tran. 55 (2012) 6391–6399.

[21] S. Zimmermann, M.K. Tiwari, I. Meijer, S. Paredes, B. Michel, D. Poulikakos, Aquasar: a hot water cooled data center with direct energy reuse, Energy 43 (2012) 237–245.
[22] B. Watson, V.K. Venkiteswaran, Universal cooling of data centres: a cfd analysis, Energy Proc. 142 (2017) 2711–2720.
[23] T. Dixit, I. Ghosh, Review of micro- and mini-channel heat sinks and heat exchangers for single phase fluids, Renew. Sustain. Energy Rev. 41 (2015) 1298–1311.
[24] A. Mohammadi, A. Koşar, Review of micro- and mini-channel heat sinks and heat exchangers for single phase fluids, Renew. Sustain. Energy Rev. 41 (2015) 1298–1311.
[25] B.W. Webb, C.F. Ma, Single-phase liquid jet impingement, Adv. Heat Tran. 26 (1995) 105–217.
[26] A.J. Robinson, E. Schnitzler, An experimental investigation of free and submerged miniature liquid jet array impingement heat transfer, Exp. Therm. Fluid Sci. 32 (1) (2007) 1–13.
[27] R. Kempers, J. Colenbrander, W. Tan, R. Chen, A.J. Robinson, Experimental characterization of a hybrid impinging microjet-microchannel heat sink fabricated using high-volume metal additive manufacturing, Int. J. Thermofluids 5–6 (2020), 100029.
[28] D. Nikolić, M. Hutchison, P.T. Raide, A.J. Robinson, Hot Spot Targeting with a Liquid Impinging Jet Array Waterblock, THERMINIC, Leuven, Belgium, 7-9 October 2009.
[29] Y. Lee, P.S. Lee, S.K. Chou, Hotspot mitigating with obliquely finned microchannel heat sink—an experimental study. Components, packaging and manufacturing technology, IEEE Trans. Compon. Packag. Technol. 3 (8) (2013) 1332–1341.
[30] C.S. Sharma, G. Schlottig, T. Brunschwiler, M.K. Tiwari, B. Michel, D. Poulikakos, A novel method of energy efficient hotspot-targeted embedded liquid cooling for electronics: an experimental study, Int. J. Heat Mass Tran. 88 (2015) 684–694.
[31] G. Laguna, M. Vilarrubí, M. Ibañez, Y. Betancourt, J. Illa, H. Azarkish, A. Amnache, L.M. Collin, P. Coudrain, L. Fréchette, J. Barrau, Numerical parametric study of a hotspot-targeted microfluidic cooling array for microelectronics, Appl. Therm. Eng. 144 (2018) 71–80.
[32] R. Wu, Y. Fan, T. Hong, H. Zou, R. Hu, X. Luo, An immersed jet array impingement cooling device with distributed returns for direct body liquid cooling of high power electronics, Appl. Therm. Eng. 162 (2019), 114259.
[33] S. Wiriyasart, P. Naphon, Heat spreading of liquid jet impingement cooling of cold plate heat sink with different fin shapes, Case Stud. Therm. Eng. 20 (2020), 100638.
[34] D. Kong, Y. Kim, M. Kang, E. Song, Y. Hong, H.S. Kim, K.J. Rah, H.G. Choi, D. Agonafer, H. Lee, A holistic approach to thermal-hydraulic design of 3D manifold microchannel heat sinks for energy-efficient cooling, Case Stud. Therm. Eng. 28 (2021), 101583.
[35] C.J.M. Lasance, How to estimate heat spreading effects in practice, J. Electron. Packag. 132 (3) (2010), 031004.
[36] Intel® Xeon® Processor Scalable Family Thermal Mechanical Specifications and Design Guide, December 2019. https://www.intel.com/content/dam/www/public/us/en/documents/guides/xeon-scalable-thermal-guide.pdf.
[37] A, M.S. El-Genk, Thermally anisotropic composite heat spreaders for enhanced thermal management of high-performance microprocessors, Int. J. Therm. Sci. 100 (2016) 213–228.
[38] S. Chevillard, The functions erf and erfc computed with arbitrary precision and explicit error bounds, Inf. Comput. 216 (2012) 72–95.
[39] J. Holland, Adaptation in Natural and Artificial Systems, The University of Michigan Press, Ann Arbor, Michigan, 1975.
[40] The MathWorks Inc, Global Optimization Toolbox User's Guide 2022a, March 2022.
[41] A.J. Robinson, A thermal-hydraulic comparison of liquid microchannel and impinging liquid jet array heat sinks for high power electronics cooling, IEEE Trans. Compon. Packag. Technol. 32 (2) (2009) 347–357.